Trajectory optimisation of an aerobatic air race

H. van der Plas and H. G. Visser
Delft University of Technology,
Delft, The Netherlands

ABSTRACT

This paper deals with the synthesis of optimal trajectories for aerobatic air races. A typical example of an air race event is the Red Bull Air Race World Series, where high-performance aerobatic aircraft fly a prescribed slalom course consisting of specially designed inflatable pylons, known as 'air gates', in the fastest possible time. The trajectory that we seek to optimise is based on such a course. The air race problem is formulated as a minimum-time optimal control problem and solved in open-loop form using a direct numerical multi-phase trajectory optimisation approach based on collocation and non-linear programming. The multiphase feature of the employed collocation algorithm is used to enable a Receding-Horizon optimisation approach, in which only a limited number of manoeuvres in sequence is considered. It is shown that the Receding-Horizon control approach provides a near-optimal solution at a significantly reduced computational cost relative to trajectory optimisation over the entire course. To avoid the path inclination singularity in the equations of motion based on Euler angles, a point-mass model formulation is used that is based on quaternions. Numerical results are presented for an Extra 300S, a purpose-designed aerobatic aircraft.

NOMENCLATURE

C_L	lift coefficient
D	aerodynamic drag
g	acceleration of gravity
h	altitude
L	lift force
n_{max}	structural load limit
p_w, q_w, r_w	reference-axes angular rate component
P	power
q_0, q_1, q_2, q_3	component of quaternion
S	wing surface area
t	time
T	thrust
V	airspeed
W	aircraft gross weight
x_g, y_g	position co-ordinates, ground-axes system
α	angle-of-attack
γ	flight path angle
$\delta(t)$	engine power setting
η_j	propulsive efficiency
μ	velocity bank angle
ρ	air density
χ	heading angle

1.0 INTRODUCTION

The first ever air race was held in 1909. The Reims Air Race ran from Reims, France to England and lasted a week. This race was won by Glenn Curtis who crossed the finish line with a five-second lead over his opponent. Curtis was crowned 'Champion Air Racer of the World'. An important catalyst for air racing in the US was the Pulitzer Trophy, announced in 1919 for international air races held in this country. The first race took place in 1920 on Long Island and was won by an American, Corliss Moseley, who averaged 156·5mph

Paper No. 3308. Manuscript received 20 June 2008, revised version received 10 September 2008, 2nd revised version received 10 November 2008, accepted 12 November 2008.

https://doi.org/10.1017/S0001924000002724 Published online by Cambridge University Press

over a closed-circuit course before a crowd of more than 25,000 spectators. That led to the establishment in 1921 of a national air meet. More competitive events were added to the programme and the meet became known as the National Air Races in 1924, which lasted to 1949.

Begun in 1964, the Reno Air Races, also known as the National Championship Air Races, take place each September at the Reno Stead near Reno, Nevada, USA. The five-day event attracts attendance totalling about 200,000. Recently, Red Bull has started sponsoring a series called the Red Bull Air Race in which competitors have to individually slalom through an obstacle course, comprising of a series of inflatable pylons known as air gates, in the fastest possible time. The Red Bull air races are quite popular, drawing vast crowds of spectators (totalling about 700,000 at the Red Bull Air Race in Rotterdam in 2005, for example) and are aired on television worldwide.

The goal of this study is to develop a tool that allows generating a time-optimal trajectory for an aerobatic air race as it is flown at, for example, the Red Bull Air Race. Although piloted simulation can be used for practicing manoeuvres and for pilot familiarisation with any course, it is evident that off-line simulation and related analysis tools have not been available for this application. The development of a trajectory optimisation tool is seen as a valuable aid for the development of air race tactics or for the assessment of competing aircraft designs.

The aerobatic air race problem can not be modelled with the 'standard' Euler equations of motion since they exhibit a singularity when the flight path reaches or passes through ±90 degrees, a situation that frequently occurs when performing aerobatic manoeuvres. For this reason, an alternative set of equations of motion is used, based on a singularity-free quaternion formulation[1,2,3].

Solving the complete problem in a single optimisation run requires a huge computational effort. For this reason, an alternative, less computationally intensive approach is explored in this paper. More specifically, the problem will be formulated as a 'Receding-Horizon' optimal control problem, where only a finite number of aerobatic manoeuvres between consecutive gate crossings are considered in a single optimisation run. The horizon length required for a satisfactory level of accuracy is assessed by comparing the Receding-Horizon optimal control solutions to the solution of the full-size problem.

2.0 PROBLEM FORMULATION

2.1 Equations of motion

Assuming that the aircraft behaves as a point mass[4], flight over a non-rotating flat earth is considered. Furthermore, it is assumed that no wind is present and that the aircraft performs a co-ordinated flight (no side-slip is present). The equations of motion are taken from Well and Wever[2]:

$$\dot{x}_g = V(q_0^2 + q_1^2 - q_2^2 - q_3^2) \quad \ldots(1)$$

$$\dot{y}_g = 2V(q_0 q_3 + q_1 q_2) \quad \ldots(2)$$

$$\dot{h} = 2V(q_0 q_2 + q_1 q_3) \quad \ldots(3)$$

$$\dot{V} = \frac{g}{W}\left(T\mathrm{Cos}\alpha - D \right) + 2g(q_1 q_3 - q_0 q_2) \quad \ldots(4)$$

$$\dot{q}_0 = -\frac{1}{2}(q_1 p_w + q_2 q_w + q_3 r_w) \quad \ldots(5)$$

$$\dot{q}_1 = \frac{1}{2}(q_0 p_w + q_2 r_w - q_3 q_w) \quad \ldots(6)$$

$$\dot{q}_2 = \frac{1}{2}(q_0 q_w + q_3 p_w - q_1 r_w) \quad \ldots(7)$$

$$\dot{q}_3 = \frac{1}{2}(q_0 r_w + q_1 q_w - q_2 p_w) \quad \ldots(8)$$

with:

$$Vr_w = 2g(q_0 q_1 + q_2 q_3) \quad \ldots(9)$$

$$Vq_w = \frac{g}{W}\left(T\,\mathrm{Sin}\alpha + L \right) - g(q_0^2 - q_1^2 - q_2^2 + q_3^2) \quad \ldots(10)$$

where x_g, y_g are the horizontal position coordinates, h the altitude, V the airspeed, q_0 , q_1 , q_2 and q_3 are the quaternion components, α is the angle-of-attack, T the thrust, D the drag and W the weight of the aircraft. The parameters p_w, q_w, r_w are the reference-axes angular rate components. Along any solution of Equations.(1) through (8), the quaternions must satisfy the constraint:

$$q_0^2 + q_1^2 + q_2^2 + q_3^2 = 1 \quad \ldots(11)$$

However, due to the nature of the quaternions it is sufficient to require satisfaction at the initial time t_0 only[1,2]. The reference-axes angular rates p_w, q_w, r_w can be related to the Euler-angles and Euler-angle rates:

$$\begin{pmatrix} p_w \\ q_w \\ r_w \end{pmatrix} = \begin{bmatrix} 1 & 0 & -\mathrm{Sin}\gamma \\ 0 & \mathrm{Cos}\mu & \mathrm{Sin}\mu\,\mathrm{Cos}\gamma \\ 0 & -\mathrm{Sin}\mu & \mathrm{Cos}\mu\,\mathrm{Cos}\gamma \end{bmatrix} \begin{pmatrix} \dot{\mu} \\ \dot{\gamma} \\ \dot{\chi} \end{pmatrix} \quad \ldots(12)$$

where μ is the bank angle, γ the flight path angle and χ the heading angle. The Euler-angles can be extracted from the quaternions:

$$\gamma = \mathrm{Arc\,sin}2(q_0 q_2 - q_1 q_3) \quad \ldots(13)$$

$$\chi = \mathrm{Arc\,tan}\left(\frac{q_0 q_3 + q_1 q_2}{\frac{1}{2} - q_2^2 - q_3^2} \right) \quad \ldots(14)$$

https://doi.org/10.1017/S0001924000002724 Published online by Cambridge University Press



Figure 1. Extra 300S aerobatic aircraft.

$$\mu = \text{Arc tan}\left(\frac{q_0 q_1 + q_2 q_3}{\frac{1}{2} - q_2^2 - q_1^2}\right) \quad \ldots(15)$$

2.2 Aircraft model

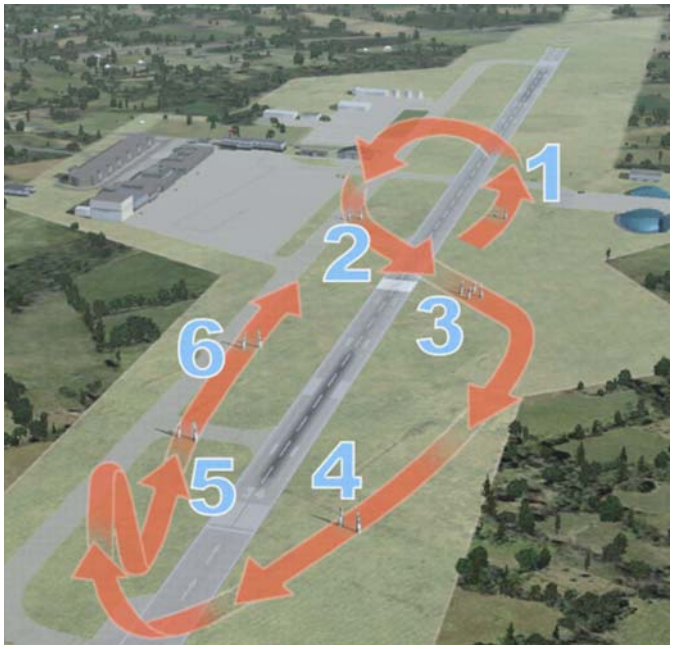
The aircraft model employed in this study is based on the Extra 300S (see Fig. 1). The Extra is a purpose-designed aerobatic aircraft, capable of competing at an international level. The aircraft is equipped with a Lycoming AE10-540-L1B5 330hp engine. The characteristics of the Extra 300S have been extracted from Microsoft *Flight Simulator X*. The most important aircraft characteristics are summarised in Table 1. The aircraft weight is assumed to remain constant throughout the entire trajectory. The assumed overall aircraft weight of 7,500N is based on the empty weight of the aircraft, plus the weight of fuel corresponding to a flight of 10 minutes of flight with full throttle, and an assumed body weight of the pilot of 800N.

2.3 Air race scenario

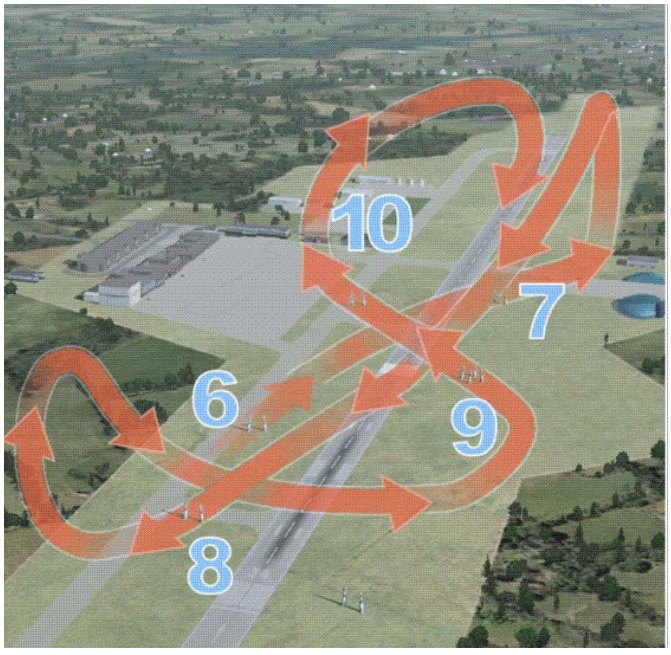
The track that the aircraft will follow is extracted from Microsoft *Flight Simulator X*, and is similar to a trajectory as flown by pilots that compete in the Red Bull Air Races. A layout of the selected example course can be found in Fig. 2. It has to be noted that the selected example course has never actually been flown by pilots. The course comprises ten air gates that each consists of one or two pairs of pylons, which stand at 20 metres high. The distance between each pair is 10-14 metres. When crossing a gate, the aircraft must fly

Table 1
Extra 300S Characteristics

Type	Extra 300S
Engine	Lycoming AE10-540-L1B5
Power (P)	330hp
Specific fuel consumption	0·08 gal/ (hp•hr)
A/C empty weight	6,100N
Maximum take-off weight	9,300N
Never exceed velocity (V_{max})	220kt
Wing surface area (S)	10·35m^2
Imposed (structural) load limit (n_{max})	±10



(a)



(b)

Figure 2. Layout of the course tracks.

either wings-level or 'knife edge' ($\mu = \pm\pi/2$), depending on the colour or the gate. In the present scenario, the aircraft must fly 'knife edge' passing through gates 3, 5, 8 and 9, and horizontal passing all other gates. After passing gates 4 and 7, the aircraft has to pull up vertically ($\gamma = \pi/2$). After the vertical-manoeuvre at gate 7, the aircraft has to perform a high-speed touch-and-go at the runway at the chalk line. All gates will be crossed horizontally ($\gamma = 0$) at a height of 10m. The minimum height that the aircraft is allowed to fly (h_{min}) is 5m. The co-ordinates and orientation of the gates can be found in Table 2. In this study, the aircraft is required to fly precisely through the centre of the gates and at the prescribed heading, to simplify the calculations. In an actual air race, deviations of at most 20 degrees are allowed without incurring a time penalty. The same holds for the bank angle μ, and here, either 0 or ±90 degrees is

https://doi.org/10.1017/S0001924000002724 Published online by Cambridge University Press

Table 2
Coordinates and orientation of the gates ($0 \le \chi \le 2\pi$)

Gate	x_g (m)	y_g (m)	h (m)	γ (rad)	χ (rad)	μ(rad)
1	0·0	–10·0	10·0	0·0	0·0	0·0
2	–148·15	165·15	10·0	0·0	4·2355	0·0
3	–316·55	–137·15	10·0	0·0	4·2355	± π/2
4	–912·7	–398·15	10·0	0·0	π	0·0
5	–869·65	–163·95	10·0	0·0	0·30871	± π/2
6	–639·75	–52·75	10·0	0·0	0·79235	0·0
7	0·0	–10·0	10·0	0·0	0·0	0·0
runway	–350·0	–51·4	0·0	0·0	3·45031	0·0
8	–869·65	–163·95	10·0	0·0	3·45031	± π/2
9	–325·95	–154·35	10·0	0·0	1·09390	± π/2
10	–148·5	–165·15	10·0	0·0	1·09390	0·0

required, whilst in a race a slight deviation is allowed without incurring penalty seconds.

2.4 Optimal control problem

The goal of the optimal control problem is to find the trajectory that minimises the flight time t_f while satisfying all operational constraints and avoiding all obstacles in accordance with the regulations. Using a generic formulation, the optimal control problem can be posed as follows:

Minimise: $J = t_f$

subject to: $\mathrm{d}\boldsymbol{z}(t)/\mathrm{d}t = f[\boldsymbol{z}(t), \mathbf{u}(t)]$, …(16)

where: $\boldsymbol{z}(t) = [x_g(t), y_g(t), h(t), V(t), q_0(t), q_1(t), q_2(t), q_3(t)]$

$\boldsymbol{u}(t) = [C_L(t), \delta(t), p_w(t)]$ …(17)

In Equation (17), $\delta(t)$ is the engine power setting, which governs the thrust T:

$$T = \delta \frac{\eta_j P}{V} \quad , \qquad \ldots(18)$$

where η_j is the propulsive efficiency and P the engine power in Watts (see Table 1). The above dynamical system is subject to a number of (operational) state/control constraints:

$$V \le V_{max} \qquad \ldots(19)$$

$$C_L \le C_{L_{max}} \qquad \ldots(20)$$

$$0 \le \delta \le 1 \qquad \ldots(21)$$

$$-2\pi \text{ sec}^{-1} \le p_w \le 2\pi \text{ sec}^{-1} \qquad \ldots(22)$$

Furthermore, a constraint on the minimum height above ground level is placed:

$$h \ge h_{min} = 5\text{m AGL} \qquad \ldots(23)$$

In addition to the above constraints, interior-point boundary conditions on the position co-ordinates x_g, y_g, and h, the bank angle μ, the flight path angle γ and the heading angle χ are enforced to ensure that the aircraft flies through the air gates, as defined in Table 2, in a correct way.

2.5 Numerical optimisation method

The numerical optimisation method employed in this study to solve the air-race problem is the direct optimisation technique of collocation with nonlinear programming (NLP). The collocation method essentially transforms an optimal control problem into a NLP formulation by discretising the trajectory dynamics[5,6]. To this end, the time interval of an optimal trajectory solution is divided into a number of subintervals. The individual time points delimiting the subintervals are called nodes. The values of the states and the controls at the nodes are then treated as a set of NLP variables. The system differential equations are discretised and transformed into algebraic equations (implicit integration). The path and control constraints imposed in the original optimal control problem are treated as algebraic inequalities in the NLP formulation. The adopted collocation approach results in piecewise constant control histories and piecewise linear state histories.

To solve the described optimal control problem, a software package called EZopt has been used[7]. As mentioned earlier, the optimal control problem is solved by discretising the time interval in smaller subintervals, thus approximating the state and control variables. Generally, the accuracy of the numerical solution of the problem improves with an increasing number of subintervals, or equivalently, the number of grid points. On the other hand, increasing the number of grid points requires a larger computational effort, hence forcing a compromise between desired accuracy and computational burden.

In addition to the collocation technique, the EZopt package also offers the capability to apply the so-called differential inclusion approach[8]. Application of this trajectory optimisation technique has also been explored. The performance of the differential inclusion technique proved to be very similar to the collocation approach.

The EZopt tool features a capability for handling multi-phase problems. A multi-phase formulation allows discontinuities at phase transitions, as well as the implementation of a different dynamic system in each phase. The multi-phase feature of EZopt is of vital importance for the optimisation procedure used in this study, since it allows enforcement of the interior boundary conditions associated to the air gates. To this end, the trajectory is split up into several flight legs, where a leg typically connects two consecutive air gates. More specifically, the air race trajectory considered here is split into twelve sequential phases, which are arranged according to the different gates through which the aircraft has to fly plus the two required manoeuvres in which the aircraft has to adopt a vertical attitude after passing through gates 4 and 7, along with the high-speed touch down at the runway between gates 7 and 8. These vertical states are denoted as ‘Vertical 4’ and ‘Vertical 7’, along with the high-speed touch down labelled as ‘Chalk line’. The arrangement of the phases is listed in Table 3.

2.6 Receding-horizon multi-phase optimisation

Optimising the 12 phases, as defined above, in a single optimisation run, results in a very large scale NLP problem (of around 2,250 NLP variables and approximately 2,150 non-linear constraints) that is

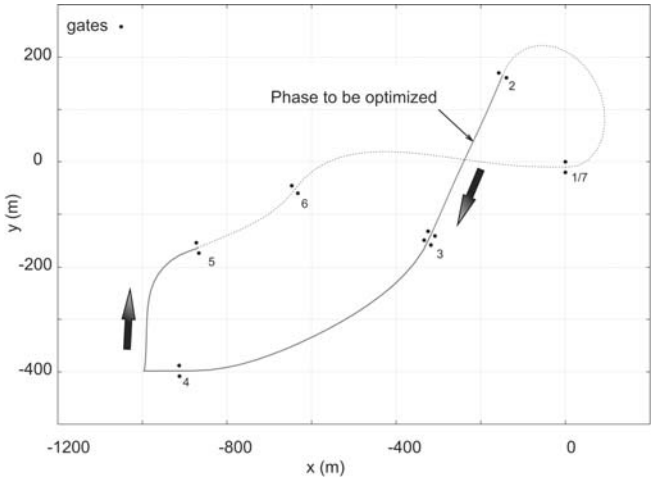
https://doi.org/10.1017/S0001924000002724 Published online by Cambridge University Press

Table 3
Arrangement of phases

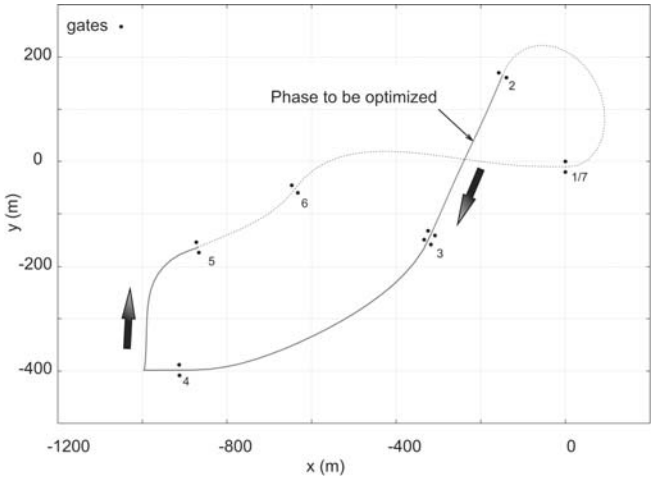
Phase	Trajectory leg
1	Gate 1 – Gate 2
2	Gate 2 – Gate 3
3	Gate 3 – Gate 4
4	Gate 4 – Vertical 4
5	Vertical 4 – Gate 5
6	Gate 5 – Gate 6
7	Gate 6 – Gate 7
8	Gate 7 – Vertical 7
9	Vertical 7 – Chalk Line
10	Chalk Line – Gate 8
11	Gate 8 – Gate 9
12	Gate 9 – Gate 10

very time consuming to solve, due to the huge computational effort that is required. In order to alleviate the computational burden, a Receding-Horizon optimisation approach is attempted[9,10]. This method breaks down the large-scale trajectory optimisation problem into several smaller sub-problems, each of which considers a limited time horizon. In general, the key issue of the Receding-Horizon approach is how to account for the part of the trajectory beyond the limited look-ahead horizon. Most Receding-Horizon methods use penalty functions added to the cost function to predict the future part of the track and to compensate the controls in the limited horizon[9,10]. In the present air race study, a Receding-Horizon multi-phase optimal control approach (which in the sequel we will refer to as the RHM) is adopted, which considers only a limited (discrete) number of phases in each evaluation, with no allowance for the future part of the trajectory that extends beyond the horizon. By selecting a horizon that covers only a discrete number of phases, an optimisation formulation is obtained in which the interior-point (air gate) boundary conditions of the full problem become the terminal boundary conditions of the limited horizon problem. It is noted that the air gate constraints do not prescribe values for all state variables and, therefore, the full problem can not be decomposed into a sequence of smaller sub-problems without loss of accuracy. The most significant state variable whose value is not prescribed at interior points is airspeed V. Errors that will accrue in the RHM approach are therefore likely to be the result of miss predictions of the values of this particular state variable at the interior points. To determine the required length of the look-ahead horizon, RHM optimal control solutions have been obtained for horizons of various sizes (covering 1 to 5 phases). A comparison of the RHM control solutions with the optimal trajectory solution for the full problem allows assessment of the accuracy of the various Receding-Horizon control solutions.

The operating principle of the RHM optimal control approach is illustrated in Fig. 3. In Fig. 3a, the evaluation of the Receding-Horizon optimal control solution for the first phase is illustrated for a horizon extending over three phases. In Fig. 3b, the solution for the second phase is shown. Phase 2 is optimised using a horizon covering phases 2 to 4 and so on. The initial conditions pertaining to the second phase problem are extracted from the first phase solution. To solve the overall 12-phase problem, twelve consecutive RHM optimal control evaluations are needed. The RHM approximation to the overall optimal trajectory solution is then obtained by assembling the twelve RHM solutions.



(a) Receding-horizon solution for first phase.



(b) Receding-Horizon solution for second phase.

Figure 3. Illustration of the Receding-Horizon approach, for a horizon extending over three phases.

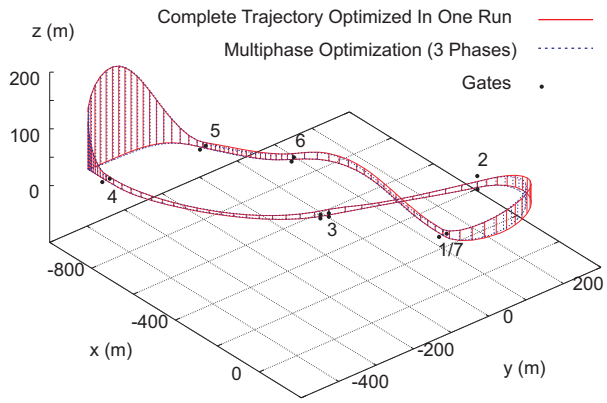
3.0 RESULTS

3.1 A comparison of a 3-phase RHM approximation to the complete time-optimal solution

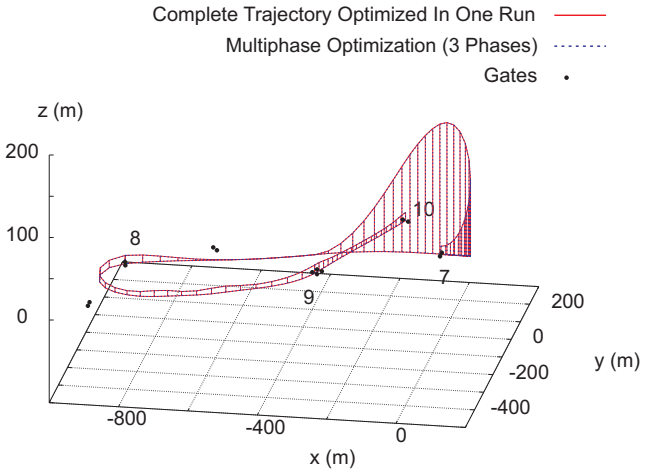
The calculation of the overall 12-phase optimal trajectory in a single run required a huge computational effort. The time needed to complete this optimisation run, based on a very good initial guess (obtained from an assembled 3-phase RHM solution), was almost 4 days with an Intel T2300 CPU (1·66GHz). The 3-dimensional presentation of the optimised flight path is given in Fig. 4 (red curves). For the sake of clarity, the presentation of the trajectory has been split up into two parts namely: gate 1 – gate 7 (Fig. 4(a)), and gate 7 – gate 10 (Fig. 4(b)). The flight time that the aircraft needs to complete the whole trajectory is 71·25 seconds. The optimal transit times per phase can be found in Table 4.

The 12-phase optimal trajectory differs from the track outline shown in Fig. 2 when the aircraft passes through gate 8. In the track layout, the proposed trajectory calls for a right turn, while in the time-optimal trajectory the aircraft turns left. The regulations do not specify a turn direction in this particular instance, and the optimisation takes advantage of this opportunity by directing a left turn.

https://doi.org/10.1017/S0001924000002724 Published online by Cambridge University Press



(a) gate 1 – gate 7 trajectory solution



(b) gate 7 – gate 10 trajectory solution

Figure 4. Comparison of a 3-Phase RHM approximation to the complete time-optimal solution.

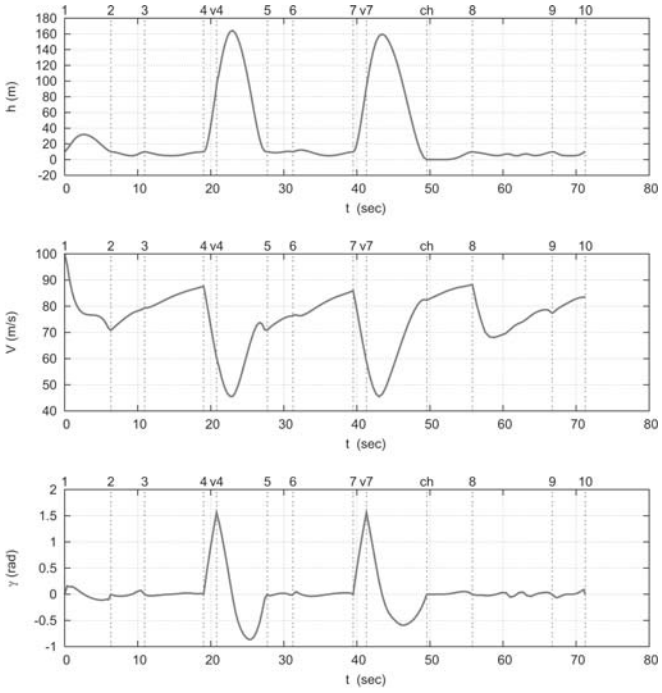


Figure 5. Trajectory Variables for the complete 12-phase time-optimal solution.

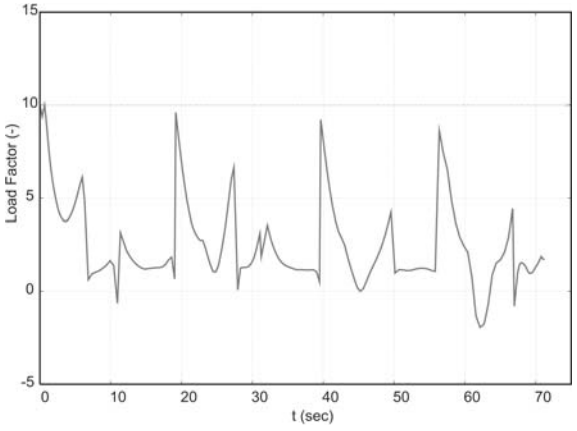


Figure 6. Time-history of load factor for the complete 12-phase time-optimal solution.

In addition to the complete 12-phase time-optimal solution, Fig. 4 also shows the assembled 3-phase RHM solution. The optimal transit times per phase for the assembled 3-phase RHM solution can also be found in Table 4. Figure 5 displays the time-histories of the most important longitudinal state variables for the complete solution.

Inspection of Fig. 4 shows that the two solutions are mostly in very close agreement. Only in the initial phase can a slight difference between the two solutions be observed. A comparison of the solutions in Fig. 4 reveals that in the 3-phase RHM approximation, the initial turn is flown much tighter and as result, the transit time is significantly lower in comparison to the complete 12-phase optimal solution. However, the tighter turn in the RHM solution also results in a lower airspeed at gate 2, which obviously is disadvantageous for the subsequent manoeuvre in phase 2. Indeed, Table 4 makes it clear that the time benefit that the RHM solution enjoys in phase 1 is completely negated in phases 2 and 3. In the subsequent phases, the differences between the solutions remain small. The overall transit time of the assembled RHM solution turns out to be marginally smaller than the 12-phase time-optimal solution. It is conjectured that this very small difference is due to discretisation errors. From these results it can be concluded that the solution obtained using the 3-phase RHM approach provides a very accurate approximation to the optimal trajectory as found by optimising all twelve phases concurrently in a single optimisation run.

Numerical experiments have shown that an increase in the horizon length does not lead to significantly better results. However, reducing the horizon length has a considerable impact on the accuracy of the approximation. This issue is explored in the next subsection.

In Fig. 6, the time-history of load factor is presented for the complete solution. It can be observed that during four of the manoeuvres the load briefly exceeds the 8g level. The structural load limit (n_{max} = 10) is only reached during the very first manoeuvre. It is noted that during the manoeuvres moderately negative load factors have been allowed to improve the solution.

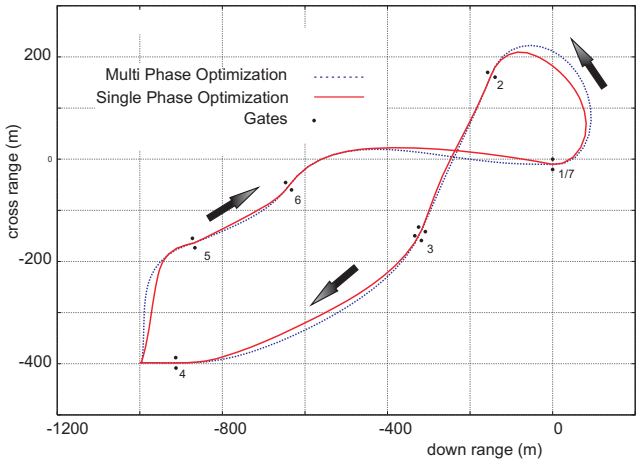
https://doi.org/10.1017/S0001924000002724 Published online by Cambridge University Press

Table 4
Comparison of transit times per phase for the 3-phase RHM and 12-phase time-optimal solutions

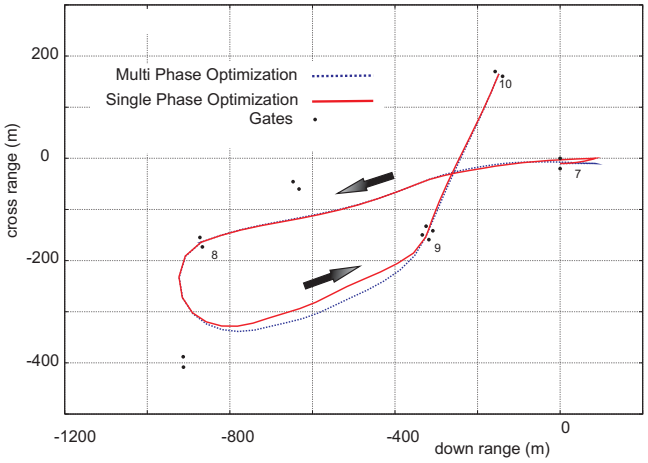
Phase	Trajectory leg	Transit time (sec) 12-phase sol.	Transit time (sec) 3-phase RHM sol
1	Gate 1 - Gate 2	6·543	6·321
2	Gate 2 - Gate 3	4·521	4·622
3	Gate 3 - Gate 4	7·984	8·075
4	Gate 4 – Vertical 4	1·792	1·778
5	Vertical 4 - Gate 5	6·973	6·955
6	Gate 5 - Gate 6	3·491	3·494
7	Gate 6 - Gate 7	8·245	8·236
8	Gate 7 – Vertical 7	1·815	1·822
9	Vertical 7 - Chalk Line	8·250	8·261
10	Chalk Line - Gate 8	6·237	6·240
11	Gate 8 - Gate 9	10·934	10·93
12	Gate 9 - Gate 10	4·521	4·518
Total		71·306	71·254

Table 5
Comparison of transit times per phase for the 3-phase RHM and single-phase solutions

Phase	Trajectory leg	Transit time (sec) Single-phase sol	Transit time (sec) 3-phase RHM sol
1	Gate 1 – Gate 2	5·963	6·321
2	Gate 2 – Gate 3	5·067	4·622
3	Gate 3 – Gate 4	8·406	8·075
4	Gate 4 – Vertical 4	1·836	1·778
5	Vertical 4 – Gate 5	6·893	6·955
6	Gate 5 – Gate 6	3·687	3·494
7	Gate 6 – Gate 7	8·517	8·236
8	Gate 7 – Vertical 7	1·890	1·822
9	Vertical 7 – Chalk Line	8·347	8·261
10	Chalk Line – Gate 8	6·297	6·240
11	Gate 8 – Gate 9	10·907	10·93
12	Gate 9 – Gate 10	4·781	4·518
Total		72·591	71·254



(a) gate 1 – gate 7 trajectory solution.



(b) gate 7 – gate 10 trajectory solution.

Figure 7. Comparison of a 3-phase RHM approximation to a single-phase solution.

Although the size of the NLP problem associated with a 3-phase RHM evaluation is only one quarter of the size of the NLP problem associated with the full 12-phase track time-optimal problem, the differences in the required computational time are far more significant. Indeed, based on a medium-quality initial guess, a single 3-phase RHM evaluation typically requires only about ten minutes of CPU time. The CPU time needed to calculate a complete assembled trajectory is about 40 minutes.

3.2 A comparison of a single-phase solution and a 3-phase RHM approximation

The near-optimal trajectory that is generated using the 3-phase RHM approach is compared to a trajectory that is obtained by sequentially optimising one phase at a time. In the latter approach, the initial conditions for a given phase are the final conditions from the preceding phase, and there is essentially no look-ahead horizon.

The results are shown in Figs. 7 and 8. Table 5 compares the transit times per phase for the two solutions. From Fig. 7 it can be observed that the aircraft again features a smaller turn radius in the single-phase solution, decreasing the distance flown. For the initial phase in the single-phase solution, this is quite beneficial in terms of the transit time (i.e., a reduction of about 0·36 seconds relative to the 3-phase RHM

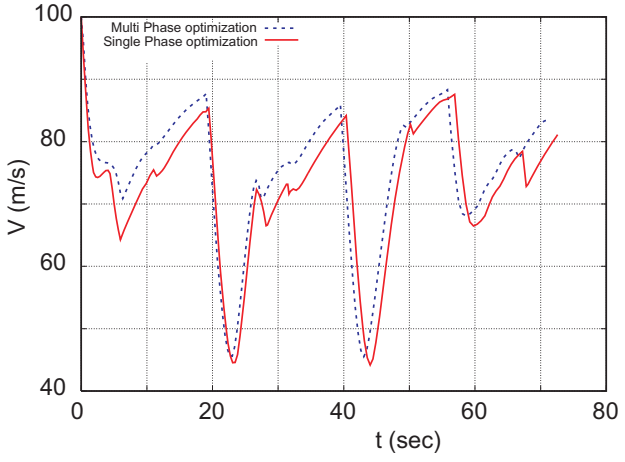


Figure 8. A comparison of airspeed time-histories of the 3-phase RHM and single-phase solutions.

https://doi.org/10.1017/S0001924000002724 Published online by Cambridge University Press



Figure 9. An aircraft competing in a Red Bull air race.

solution), however, this comes at the cost of a significantly reduced airspeed (see Fig. 8) at the start of phase 2. The reduced airspeed at the start at phase 2 (of about 4 m/s) results in a significant increased transit time for phases 2 and 3, to the extent that at the end of phase 3 the initial benefit is more than offset so that ultimately, a net increase in transit time of about 0.42 seconds is sustained. In the subsequent manoeuvres this pattern of events is repeated: the turns are tighter in the single-phase solution, but the associated increased bleed-off of speed results in larger transit times for the subsequent (wings-level) acceleration phases. This ultimately leads to an increase in flight time of about 1·34 seconds (or 1·9%) for the complete track, relative to the optimal solution, which is certainly significant.

4.0 CONCLUSION

The goal of this study was to find an optimal trajectory for a series of aerobatic manoeuvres, typically found in an air race. By using a quaternion formulation, the singularity in the standard Euler equations was avoided and the optimal control computations were greatly simplified. To make the problem computationally tractable, a Receding-Horizon Multi-phase (RHM) optimal control formulation was employed. It was found that only a limited look-ahead horizon is needed to assemble a near-optimal trajectory. Calculating the time-optimal solution for the entire course in a single run proved to be a very tedious affair. Although we ultimately were able to obtain a converged solution for the full problem, we managed to do so only after we had first established a very good initial guess, based on an assembled 3-phase RHM solution. The computational effort required to calculate an assembled 3-phase RHM solution turned out to be only a fraction (i.e., about 1/150) of the computational cost needed for the full solution (at least, in the presently considered computational environment). The developed trajectory optimisation tool holds out great promise to be used as an aid in developing air race tactics or in the assessment of competing aircraft designs.

In the present air race formulation, a no-wind condition has been assumed. In the near future, the research will be extended to include the effect of wind in the equations of motion.

REFERENCES

1. WUENSCHE, H. Singularity-free Methods for Aircraft Flight Path Optimization Using Euler Angles and Quaternions, Master's thesis, Aerospace Engineering Department, University of Texas, Austin, Texas, USA, 1982.
2. WELL, K.H. and WEVER, U.A. Aircraft trajectory optimization using quaternions — comparison of a nonlinear programming and a multiple shooting approach, Proceedings IFAC 9th Triennial World Congress, Budapest, Hungary, 1984, pp 1595-1602.
3. STEVENS, B.L. and LEWIS, F.L. *Aircraft Control and Simulation,* John Wiley & Sons, Toronto, Canada, 1992.
4. RUIJGROK, G., *Elements of Airplane Performance,* Delft University Press, Delft, The Netherlands, 1996.
5. BRINKMAN, K. and VISSER, H.G. Optimal turn-back maneuver after engine failure in a single-engine aircraft during climb-out, Proceedings of the Institution of Mechanical Engineers — Part G, *J Aero Eng,* 2007, **221,** (1), pp 17-27.
6. VISSER, H.G. and WIJNEN, R.A.A. Optimization of noise abatement departure trajectories, *J Aircr*, July-August 2001, **38,** (4), pp 620-627.
7. SEYWALD, H. and KUMAR, R. *EZopt: An Optimal Control Toolkit,* Analytical Mechanics Associates, Hampton, VA, USA, 1997.
8. SEYWALD, H. Trajectory optimization based on differential inclusion, *J Guidance, Control and Dynamics,* May — June 1994, **17,** (3), pp 480-487.
9. MAYNE, D.Q. and MICHALSKA, H. Receding horizon control of nonlinear systems, *IEEE Transactions on Automatic Control,* July 1990, **35,** (7), pp 814-824.
10. CRASSIDIS, J.L., MARKLEY, F.L., ANTHONY, T.C. and ANDREWS, S.F. Nonlinear predictive control of spacecraft, *J Guidance, Control and Dynamics,* November — December 1997, **20,** (6), pp 1096-1103.

https://doi.org/10.1017/S0001924000002724 Published online by Cambridge University Press